PCCP

PAPER

View Article Online
View Journal | View Issue

Cite this: *Phys. Chem. Chem. Phys.*, 2024, **26**, 16529

Conformational control of antimicrobial peptide amphiphilicity: consequences for boosting membrane interactions and antimicrobial effects of photocatalytic TiO_2 nanoparticles†

Lucrezia Caselli, ‡*[a] Sebastian Köhler,[b] Davide Schirone,[c] Ben Humphreys[d] and Martin Malmsten [ae]

This study reports on the effects of conformationally controlled amphiphilicity of antimicrobial peptides (AMPs) on their ability to coat TiO_2 nanoparticles (NPs) and boost the photocatalytic antimicrobial effects of such NPs. For this, TiO_2 NPs were combined with AMP EFK17 (E**F**KR**I**VQR**I**KD**F**LRNLV), displaying a disordered conformation in aqueous solution but helix formation on interaction with bacterial membranes. The membrane-bound helix is amphiphilic, with all polar and charged amino acid residues located at one side and all non-polar and hydrophobic residues on the other. In contrast, the d-enantiomer variant EFK17-d (E(d**F**)KR(d**I**)VQR(d**I**)KD(d**F**)LRNLV) is unable to form the amphiphilic helix on bacterial membrane interaction, whereas the W-residues in EFK17-W (E**W**KR**W**VQR**W**KD**F**LRNLV) boost hydrophobic interactions of the amphiphilic helix. Circular dichroism results showed the effects displayed for the free peptide, to also be present for peptide-coated TiO_2 NPs, causing peptide binding to decrease in the order EFK17-W > EFK17 > EFK17-d. Notably, the formation of reactive oxygen species (ROS) by the TiO_2 NPs was essentially unaffected by the presence of peptide coating, for all the peptides investigated, and the coatings stabilized over hours of UV exposure. Photocatalytic membrane degradation from TiO_2 NPs coated with EFK17-W and EFK17 was promoted for bacteria-like model bilayers containing anionic phosphatidylglycerol but suppressed in mammalian-like bilayers formed by zwitterionic phosphatidylcholine and cholesterol. Structural aspects of these effects were further investigated by neutron reflectometry with clear variations observed between the bacteria- and mammalian-like model bilayers for the three peptides. Mirroring these results in bacteria-like model membranes, combining TiO_2 NPs with EFK17-W and EFK17, but not with non-adsorbing EFK17-d, resulted in boosted antimicrobial effects of the resulting cationic composite NPs already in darkness, effects enhanced further on UV illumination.

Received 26th April 2024,
Accepted 21st May 2024

DOI: 10.1039/d4cp01724b

rsc.li/pccp

Introduction

Photocatalytic nanoparticles (NPs) attract intense current interest as antimicrobial agents and therapeutics due to their potent and wide-spectrum effects, particularly against bacteria resistant to antibiotics.[1–3] The origin of such effects is the excitation of electrons in photocatalytic NPs by light, resulting in free electrons and positively charged holes able to react with water, dissolved oxygen, and other solutes at the NP surface. This, in turn, results in the production of reactive oxygen species (ROS), which are able to degrade essential components in bacteria, including membrane lipids, essential proteins, or DNA. Despite numerous reports in the literature demonstrating potent antimicrobial effects by photocatalytic NPs, some key issues prevent them from being further developed for antimicrobial therapeutics. Among these, the selectivity between bacteria

[a] *Department of Physical Chemistry 1, Lund University, SE-22100 Lund, Sweden. E-mail: caselli@csgi.unifi.it*
[b] *LINXS Institute of Advanced Neutron and X-ray Science, Scheelevagen 19, 22370 Lund, Sweden*
[c] *Department of Biomedical Sciences and Biofilms-Research Center for Biointerfaces (BRCB), Malmö University, 20506 Malmö, Sweden*
[d] *Institut Laue–Langevin, CS 20156, 38042 Grenoble Cedex 9, France*
[e] *Department of Pharmacy, University of Copenhagen, DK-2100 Copenhagen, Denmark*

† Electronic supplementary information (ESI) available: Calculated SLDs, summaries of structural data obtained from NR experiments, NR curves and best fits, data on oxidation kinetics, QCM kinetics results, as well as CD results and fittings. This material also includes input parameters used for NR fits and structural parameters obtained from NR fits. See DOI: **https://doi.org/10.1039/d4cp01724b**

‡ Current affiliation: Department of Chemistry "Ugo Schiff", University of Florence and CSGI, Florence, Italy.

and human cells remains a key challenge, as photocatalytic NPs may also degrade human cell membranes and other essential components, resulting in toxicity effects.[3] Addressing this, we previously demonstrated that photocatalytic TiO_2 NPs coated with antimicrobial peptides (AMPs[4–6]) may be used to enhance NP binding to bacterial membranes, thereby increasing the probability of ROS generated during illumination reaching the bacterial membrane during their short lifetime.[7]

Although previous studies demonstrate that AMP coatings can be used to selectively boost the antimicrobial effects of photocatalytic NPs, it is unclear how the properties of peptides influence membrane interactions and antimicrobial effects. This is unfortunate since much is known about how AMP properties such as charge, amphiphilicity, length, and secondary structure affect membrane interactions and antimicrobial effects for free peptides in solution. This knowledge could potentially be used to optimize the antimicrobial effects and selectivity of AMP-coated photocatalytic NPs.[4–6] Attachment to a particle surface is, however, expected to reduce conformational and translational freedom of AMPs. Since membrane destabilization and antimicrobial effects of AMPs depend critically on their ability to insert into the lipid membranes, it thus remains unclear if knowledge of peptide properties for free AMPs in solution can be used for optimizing membrane interactions and antimicrobial effects of AMP-coated photocatalytic interactions. In a first investigation into this, we reported on the effect of hydrophobic W-tags for TiO_2 NPs coated with the AMP KYE21 and its variant KYE21WWW.[8] Mirroring the results obtained for the free peptides in solution,[9] hydrophobic W-tagging resulted in AMP-coated TiO_2 NPs displaying denser and more highly cationic peptide coatings, promoting binding of the peptide-coated NPs to anionic bacteria-like phospholipid membranes. Since the W-tagging did not detrimentally influence either ROS formation or the susceptibility of the peptide coating to oxidative degradation, the higher membrane binding by KYE21WWW-TiO_2 resulted in promoted membrane degradation and antimicrobial effects. However, some saturation in photocatalytic effects was observed at very high binding densities, inferred to be due to diffuse light scattering effects.

In the present study, we focus on the role of AMP secondary structures on peptide performance as surface coatings of photocatalytic NPs for boosting bacterial membrane destabilization and antimicrobial effects. In doing so, we investigate AMP EFK17 (EFKRIVQRIKDFLRNLV), displaying a disordered structure in aqueous solution but helix formation on binding to bacterial membranes.[10,11] Importantly, the helix formed on membrane interaction is amphiphilic, with all charged/polar residues on one side, and all non-polar/hydrophobic residues on the other (Scheme 1). The conformational change induced on peptide binding to bacterial membranes is thus strongly interlinked to the amphiphilicity of the peptide. Given this, it is also possible to suppress conformationally induced peptide amphiphilicity by replacing selected amino acids in EFK17 with the corresponding D-amino acid enantiomers (EFK17-d; E(d**F**)KR(d**I**)VQR(d**I**)KD(d**F**)LRNLV). Alternatively, the overall peptide amphiphilicity can be strengthened by replacing the same residues by more hydrophobic W residues (EFK17-W; E**W**KR**W**VQR**W**KD**F**LRNLV), boosting the amphiphilicity of the helix. We previously demonstrated that the D-amino acid substitutions in EFK17 efficiently suppressed amphiphilic helix formation, thereby suppressing peptide binding to, and destabilization of, bacterial membranes. W-substitutions, on the other hand, promoted membrane binding and antimicrobial effects.[10–12] Considering this, we selected EFK17, EFK17-d, and EFK17-W as surface coatings of photocatalytic TiO_2 NPs to elucidate if conformational amphiphilicity strongly influencing bacterial membrane interactions and antimicrobial effects for the free peptides, translates to similar effects for peptides bound to the NP surface. Regarding photocatalytic NPs, we chose to work with TiO_2 NPs. Although the wide band gap for TiO_2 NPs requires UV illumination for photocatalytic effects,[13] which may be a disadvantage in some applications, it also allows excellent experimental control. Thus, normal laboratory light conditions effectively correspond to "in darkness" conditions, allowing particle–membrane interactions to be investigated in detail, whereafter oxidation effects can be conveniently "turned on" by UV illumination. Benefiting from such experimental control, detailed investigations were performed regarding NP and coating properties (peptide conformation, coating interference with ROS generation, and coating susceptibility to ROS-induced degradation), as well as how these properties influence NP binding to, and destabilization of, bacteria-like and human cell-like lipid model membranes.[14–17] We also investigated to what extent results obtained in such model studies translated into antimicrobial effects. In doing so, all experiments were

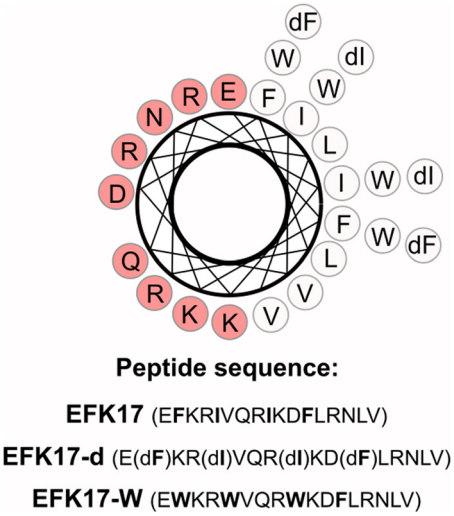

Scheme 1 Helical wheel projection of the peptide EFK17 with highlighted enantiomeric (d*F* and d*I*) and tryptophan (W) substitutions. Red and white circles represent charged (and hydrophilic) and uncharged (and hydrophobic) residues, respectively. As seen, EFK17 and EFK17-W are both able to form perfectly amphiphilic helices, with all polar/charged residues on one side and all non-polar/hydrophobic, on the other. Due to the W-substitutions, the amphiphilicity of the helix is higher for EFK17-W than for EFK17. As a result of the d-amino acid substitutions, EFK17-d is unable to form the amphiphilic helix, instead displaying disorder conformation, both in the absence and presence of membranes and TiO_2 NPs.

performed at pH 5.4, chosen to represent conditions relevant to skin infections.[18,19]

Materials and methods

Materials

TiO_2 nanoparticles (anatase, 4–8 nm) were purchased from PlasmaChem GmHb (Berlin, Germany), while EFK17 (EFKRIV QRIKDFLRNLV), EFK17-d (EFKRIVQRIKDFLRNLV) and EFK17-W (EWKRWVQRWKDWLRNLV) (all >95%) were from Thermo Fisher Scientific (US). Palmitoyloleoylphosphocholine (POPC), palmitoylarachidonoyl phosphocholine (PAPC), (palmitoyloleoylphosphoglycerol) (POPG), and cholesterol (bovine, Chol) (all >99% purity) were purchased from Avanti Polar Lipids (Alabaster, US), while C11-BODIPY 581/591 was from Molecular Probes/Thermo Fisher Scientific (US). MilliQ water (MQ, 18.2 MΩ cm) and D_2O (99% deuterated, Sigma Aldrich) were used throughout the experiments. All other chemicals were of analytical grade.

Liposome preparation

Liposomes were prepared as described previously.[20] In brief, 10 mg mL^{-1} lipid solutions in chloroform (for POPC and PAPC) or chloroform/methanol (3/1 vol%) (for POPG) were prepared in dark glass vials to 75/25 mol% POPC/PAPC ('PC'), 50/25/25 mol% POPC/PAPC/POPG ('+PG'), or 65/25/10 mol% POPC/PAPC/Chol ('+Chol') (for ROS generation and neutron reflectometry (NR) studies), or to corresponding systems with PAPC replaced by POPC (for quartz crystal microbalance with dissipation monitoring (QCM-d) and circular dichroism (CD) studies). The solvent was evaporated under N_2 and then under vacuum. The resulting films were hydrated with MilliQ water (to form supported lipid bilayers), or 10 mM acetate buffer, at pH 5.4 (for ROS and CD studies). The resulting multilamellar vesicles were tip sonicated (UP50H, Hielscher Ultrasonics GmbH, Germany (50 W, 30 kHz) used in an intermittent-pulse mode (5 s), at 100% amplitude) for 15 minutes in an ice bath to obtain small unilamellar vesicles (SUV; for supported bilayers), or extruded 30 times through polycarbonate filters (Ø 100 nm, LipoFast miniextruder (Avestin, Ottawa, Canada)) to obtain large unilamellar vesicles (LUV; for ROS and CD studies).

Preparation of peptide-coated TiO_2 NPs

To prepare peptide-coated TiO_2 NPs, EFK17, EFK17-d and EFK17-W peptides were dissolved in 1 mL of 10 mM acetate buffer, pH 5.4, at the desired concentration (from 5 to 100 μM), from 1 mM peptide stock solutions in MilliQ. 20 μL of bare TiO_2 NPs were subsequently added from a concentrated stock dispersion (5000 ppm TiO_2 in 10 mM acetate buffer, pH 5.4) under continuous stirring to obtain a 100 ppm TiO_2 NP dispersion (for live/dead bacterial viability assay, 40 μL of bare TiO_2 NPs were used instead to obtain a final TiO_2 concentration of 200 ppm in the mixed peptide/NP dispersion, to be diluted down to 100 ppm upon mixing with bacteria). Following this, pH of the dispersion was adjusted to 9.4, where TiO_2 NPs display a negative surface charge,[7] to promote binding with positively charged peptides. The dispersions were subsequently tip-sonicated (UP50H, Hielscher Ultrasonics GmbH, Germany (50 W, 30 kHz) in an intermittent-pulse mode (5 s), at 100% amplitude) for 15 minutes in an ice bath. After that, pH was lowered back to 5.4, and peptide-coated TiO_2 NPs were further tip sonicated for 15 minutes as described above. The so-obtained NP dispersions (100 ppm) were used without further modifications for dynamic light scattering and ζ-potential measurements, as well as for ROS generation assays and circular dichroism experiments. In contrast, NPs were diluted down to 20 ppm for NR measurements, or 5 ppm for QCM-d.

Size and ζ-potential measurements

Dynamic and electrophoretic light scattering (DLS and ELS; 173° back-scattering angle) were carried out with a Zetasizer Nano ZSP (Malvern Pananalytical Ltd, Malvern, UK) to obtain particle size and ζ-potential. Measurements were performed in triplicate at 25 °C using automatic attenuation. The results are reported as number-average effective particle diameters. Samples were measured within 2 hours of preparation. Within this timeframe, stable size and ζ-potential values were recorded for TiO_2 NPs coated with EFK17, EFK17-d and EFK17-W. For longer times from sample preparation and room temperature storage, aggregation of particles coated with EFK17, EFK17-d (but not with EFK17-W) starts to be observed. Such longer-term aggregation can be suppressed by storing samples at 4 °C, for longer usage. Alternatively, tip-sonication (UP50H, Hielscher Ultrasonics GmbH, Germany (50 W, 30 kHz) used in an intermittent-pulse mode (5 s), at 100% amplitude) allows for recovering efficient dispersion.

C_{11}-BODIPY 581/591 oxidation assay

ROS generation under UV illumination was investigated as described previously.[20] C_{11}-BODIPY 581/591 was incorporated into PC, +Chol and +PG LUV by adding 0.5 mol% of the probe prior to lipid film drying, keeping it under an Ar atmosphere. After vesicle formation, LUVs were illuminated by UV (Spectroline ENF-260C, 254 nm; 3 mW cm^{-2}, sample-lamp distance ~6 cm) in the presence peptide-coated TiO_2 NPs. Fluorescence spectra (λ_{ex} = 485 nm; λ_{em} = 500–700 nm) were acquired using a Cary Eclipse fluorescence spectrophotometer with a Xe pulse lamp (Agilent Technologies, USA). Oxidation was quantified from the spectral shift of the probe emission. All measurements were performed in triplicate at 25 °C.

Quartz crystal microbalance with dissipation monitoring (QCM-d)

QCM-d measurements were performed using a QSense analyzer with UV-transparent sapphire window modules (Biolin Scientific, Sweden). Cells and tubing were cleaned by bath sonication in a 2% Hellmanex solution, followed by MilliQ water and ethanol. SiO_2 surfaces (QSense QSX 303 SiO_2, 4.95 ± 0.05 MHz) were washed in Hellmanex 2%, followed by MilliQ water and ethanol, and dried with N_2. Then they were plasma cleaned for 10 minutes (Model PDC-32G, Harrick Plasma, USA) and were

mounted into the measurement cells without further modification. A liquid flow of 0.1 mL min^{-1} was employed throughout the experiments. Lipid bilayers were prepared by SUV deposition on SiO_2 surfaces as previously described.[20] In brief, SUVs (0.1 mg mL^{-1} in MQ) were injected using a peristaltic pump, followed by rinsing with MilliQ to remove excess non-adsorbed vesicles. Full vesicle rupture and bilayer formation were confirmed by changes in frequency (ΔF) of ~ -23 Hz and dissipation (ΔD) of $\sim 0.2 \times 10^{-6}$. Then, the bilayer was rinsed with buffer (10 mM Acetate, pH 5.4) and peptide-coated TiO_2 NPs were subsequently added. Right after, the buffer was flushed for 10 minutes to remove NP excess. Finally, buffer flow was stopped and samples were illuminated by UV light (Spectroline lamp ENF-260C, 6 W, 254 nm; 3 mW cm^{-2}, placed at ~ 2 cm from the QCM-d cell) for 2 h. Measurements were performed at 25 °C in triplicate.

Circular dichroism (CD)

CD spectra of 100 ppm peptide-coated TiO_2 NPs (at 50 μM peptide concentration) in 10 mM acetate (pH 5.4) were recorded in the absence and in the presence of PC, +Chol and +PG unilamellar vesicles (100 μM lipid). The CD spectra for such samples contain contributions from both free peptides and peptides bound to the TiO_2 NPs. To reduce contributions from free peptide, compositions were selected to correspond to contain the lowest possible amounts of peptide that display efficient NP dispersion. Spectra of free peptides in the same buffer were also collected as control samples. The CD signal of each sample was recorded in 1 mm path length quartz cuvettes (110-QS; Hellma, Mullheim, Germany) using a JASCO (Tokyo, Japan) J-715 CD instrument, working with 20 nm min^{-1} scanning speed, 2 s response time, and 5 nm bandwidth. The signal was collected in the 200–260 nm wavelength range as an average of 10 accumulations. The measurements were performed at 20 °C in triplicate. The mean residual ellipticity (MRE) for each sample was then obtained after subtracting the background (10 mM acetate, pH 5.4). CD spectra were subsequently analyzed using software BeStSel[21] for quantification of α-helix content.

Neutron reflectometry (NR)

NR experiments on supported +PG and PC bilayers interacting with EFK17-W-coated TiO_2 NPs were performed on the D17 vertical reflectometer (Institute Laue-Langevin, Grenoble, France), operating in the time-of-flight mode.[22,23] The Q-region of interest (0.007 to 0.3 $Å^{-1}$) was accessed using two incident angles (0.8° and 3.0°), using the wavelength range between 2 and 30 Å and wavelength resolution between 1 and 4%. The reflected intensity was acquired as a function of the momentum transfer $q_z = (4\pi/\lambda)\cdot\sin(\vartheta)$, where λ is the wavelength and ϑ is the incident angle. Solid–liquid flow cells with a top plate characterized by a 40 mm diameter circular opening were employed in combination with UV-transparent quartz blocks (80 × 50 × 15 mm, 1 face polished, RMS < 4.5 Å, PI-KEM Ltd, Tamworth, UK) to allow *in situ* UV irradiation. HPLC tubing, PEEK troughs, and O-rings were cleaned with a 2% Hellmanex (Hellma Analytics, UK) solution in MilliQ under bath sonication, then thoroughly rinsed and sonicated in MilliQ. Cells were connected to a circulating water bath to keep them at a constant temperature of 25 °C during the measurements. Before mounting them into the liquid flow cells, NR blocks were cleaned in piranha solution (5/4/1 $H_2O/H_2SO_4/H_2O_2$) at 80 °C for 15 minutes (**Caution**: Piranha solution is highly corrosive), rinsed in MilliQ, and cleaned through plasma cleaning for 15 minutes (Harrick Plasma PDC-002, USA). After that, blocks were mounted in the solid–liquid flow cells and characterized in D_2O and MilliQ H_2O. Then, PC or +PG SUV dispersions (0.1 mg mL^{-1}) were injected manually (right after tip-sonication) and allowed to deposit for 20 min. Excess SUV was subsequently rinsed off with 20 mL MilliQ water at 2 mL min^{-1}, followed by buffer (10 mM acetate, pH 5.4) rinsing at 2 mL min^{-1}. The bilayers thus formed were characterized in three contrasts, *i.e.*, d-, qm- and h-buffer, corresponding to 10 mM acetate buffer in D_2O, 68.6/31.4% v/v D_2O/H_2O mixture (with the same scattering length density (SLD) as quartz), and H_2O, respectively. Contrasts were exchanged by pumping 20 mL of the desired buffer at 2 mL min^{-1}. Subsequently, EFK17-W-TiO_2 NPs (20 ppm) in h-buffer were injected manually and incubated for 10 minutes with the bilayer. Following this, h-buffer was flushed to remove excess NPs and the reflectivity was acquired in h-, qm- and d-buffers. The bilayers were then subjected to *in situ* UV irradiation (Spectroline lamp ENF-260C, 6 W, 254 nm; 3 mW cm^{-2}) for 2 h, with the UV lamp placed at ~ 2 cm from the NR cell. After UV exposure, reflectivity curves were measured in d, qm- and h-buffers. Quantitative information about the scattering length density profile of the sample normal to the interface can be obtained through data fitting. Experimental NR profiles were fitted by using the genetic optimization method using the analysis package Motofit, available within the software IGOR Pro.[24,25] A series of parallel layers were used to model the interfacial structure, each of these described by thickness, roughness, hydration, and SLD. Monte Carlo error analysis allowing for refitting data 100 times was employed to quantify the uncertainty associated with data fitting.[26]

Live/dead bacterial viability assay

E. coli ATCC 25922 were stained using the live/dead BacLight Bacterial Viability Kit (Thermo Fisher Scientific Inc., Waltham, USA). Bacteria were grown to the stationary phase in 25 mL Lennox broth (LB Broth; Sigma Aldrich (St. Luis, USA)) under shaking at 180 rpm overnight at room temperature. After that, bacteria were pelleted and washed by centrifugation (10 000 × *g*, 10 min, twice) and finally re-suspended in 10 mM acetate, pH 5.4. Nanoparticle dispersions (500 μL), either bare or coated with EFK17, EFK17-d or EFK17-W were added to 500 μL of bacteria suspensions. NPs had a 100 ppm concentration in the final mixture, while the optical density OD600 of the bacterial dispersion was 1.2, corresponding to 12×10^8 *E. coli* colony forming units (CFU) mL^{-1} (confirmed on subsequent dilution, plating, culture, and counting of colonies). Samples were transferred to quartz cuvettes and incubated for 1 h at 25 °C, either in darkness or under UV illumination (Spectroline ENF-260C, 254 nm; 3 mW cm^{-2}), applied at a cuvette-lamp distance of 6 cm. Samples were subsequently diluted in the buffer to obtain an OD600 of 0.6, corresponding to 6×10^8 CFU mL^{-1}

E. coli. Right after, 200 μL of samples were mixed with 0.5 μL of a 1/1 (v/v) mixture of the fluorescent probes SYTO 9 (excitation/emission maxima 480/500 nm) and propidium iodide (excitation/emission maxima 490/635 nm).[27] After 10 minutes incubation, samples were imaged by confocal microscopy. Bacteria in the absence or in the presence of NPs were plated onto a cover slide at 108 CFU mL^{-1} and then imaged with a 100×/1.25″ oil objective using a Leica DMi8 confocal microscope (Leica Microsystems, Washington, DC, USA). For each sample, 20 randomized, wide-field images (100 μm × 100 μm) were collected. Quantification of the fraction of live/dead bacteria was performed using the software ImageJ (National Institutes of Health, Bethesda, USA).[28,29] Experiments were performed in triplicate at 25 °C.

Results

Properties of peptide-TiO_2 composite nanoparticles

With an isoelectric point of 6–6.5,[30,31] TiO_2 NPs only carry a modest positive charge (+5 ± 1 mV) at pH 5.4 and are therefore, colloidally unstable at this pH, as seen from very large effective particle sizes (Fig. 1A). For EFK17-W, the concentration-dependent peptide binding to the TiO_2 NPs is clearly shown from the positive ζ-potential increase, reaching +24 ± 1 mV at the highest peptide concentration investigated. As a result of the build-up of the positive ζ-potential, the TiO_2 NPs are colloidally stabilized on the peptide coating, seen from a much smaller average particle size of 147 ± 16 nm at peptide concentrations of 50 mM and above. Keeping in mind that the primary particle size for the fully dispersed TiO_2 NPs is 2–8 nm,[7] each composite NP contains multiple TiO_2 NPs which have an outer region dominated by the peptide. While a minor increase in positive ζ-potential and a minor decrease in effective particle diameter is observed as a function of EFK17d and EFK17-d concentrations, the binding of these peptides to the TiO_2 NPs is too weak to allow colloidal stabilization of the aggregating TiO_2 NPs.

Since peptides will ultimately degrade when exposed to ROS,[32,33] the susceptibility of the systems to photocatalytic degradation was investigated by monitoring the ζ-potential as a function of UV exposure. As seen in Fig. 1B, all systems displayed a minor decrease in the positive ζ-potential with increasing UV exposure time, indicating that peptide oxidation occurred. Quantitatively, however, this decrease in ζ-potential was relatively minor, suggesting that the peptide coatings are relatively robust to photocatalytic degradation over the 2 h exposure time investigated. While the AMP coatings on the TiO_2 NPs are essential for enhanced and controlled NP binding to bacterial membranes, it is possible that these coatings prevent UV-induced free electrons and holes generated during UV illumination from reaching the aqueous solution for ROS generation.

Addressing this, we investigated how the peptide coating affected ROS generation.

As seen in Fig. 2 and Fig. S1 (ESI†), free TiO_2 displays slightly higher ROS generation than either EFK17-TiO_2, EFK17-d-TiO_2, or EFK17-W-TiO_2. These minor differences could be ascribed to ROS suppression caused by the peptide shell, as well as to

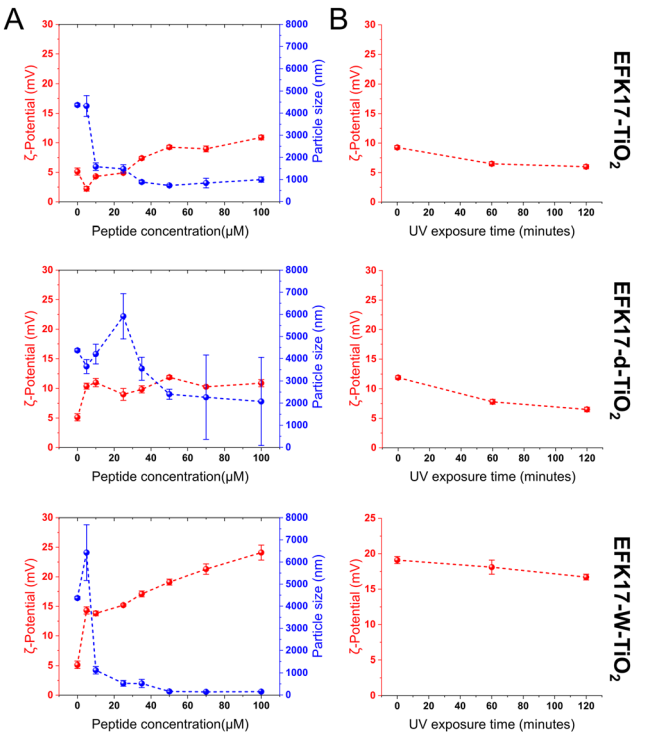

Fig. 1 Characterization of peptide-coated TiO_2 NPs. (A) ζ-potential and average particle size of TiO_2 NPs (100 ppm) loaded at varying concentrations of EFK17 (top), EFK17-d (middle) and EFK17-W (bottom) in 10 mM Acetate, pH 5.4. (n = 3); (B) ζ-potential of TiO_2 NPs coated with 50 μM EFK17 (top), EFK17-d (middle) and EFK17-W (bottom), before and after 1 or 2 h of UV illumination, in 10 mM Acetate, pH 5.4. (n = 3). Samples were characterized within 2 hours from preparation.

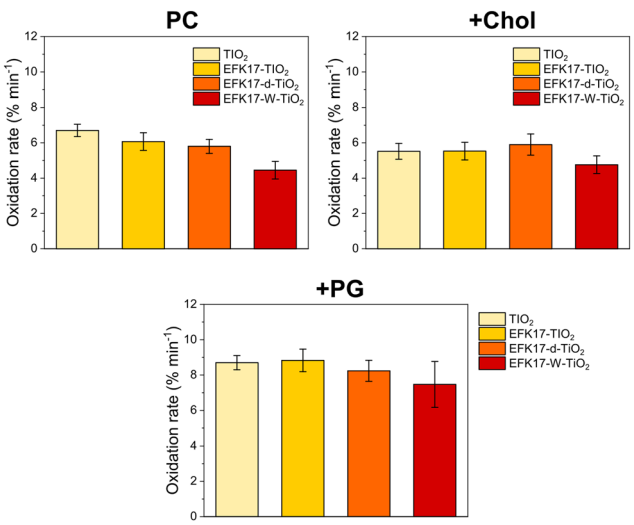

Fig. 2 C_{11}-BODIPY oxidation rates for bare TiO_2 NPs, as well as for TiO_2 NPs coated with EFK17, EFK17-d, or EFK17-W on PC (top left), +Chol (top right), and +PG (bottom) LUVs subjected to *in situ* UV exposure in 10 mM Acetate, pH 5.4. (n = 3). Corresponding oxidation kinetics are shown in Fig. S1 (ESI†).

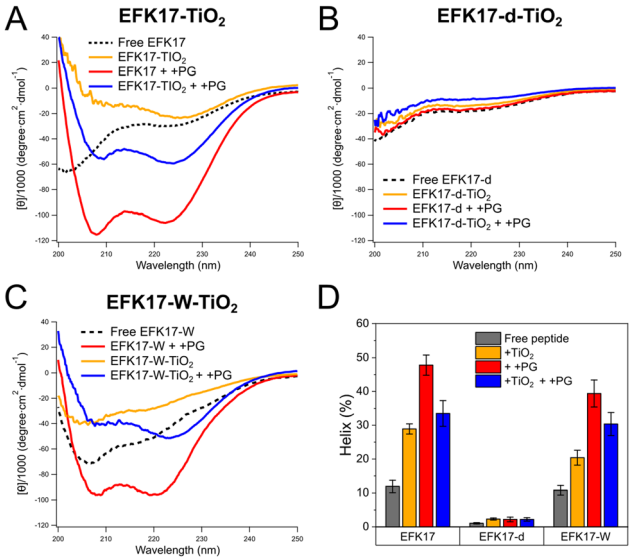

Fig. 3 CD spectra of TiO_2 NPs coated with EFK17 (A), EFK17-d (B), and EFK17-W (C) in the absence and the presence of +PG LUVs. CD spectra of free peptides and peptides incubated with +PG LUVs (in the absence TiO_2 NPs) are also included for comparison. Shown in (D) are results on alpha helix content (%) obtained from CD spectral fitting through the Bestsel method.[21] All measurements were performed at 25 °C, in 10 mM Acetate, pH 5.4. (n = 3). Corresponding results obtained for TiO_2 NPs coated with EFK17, EFK17-d and EFK17-W interacting with PC and +Chol LUVs are reported in Fig. S2 and S3 (ESI†), respectively.

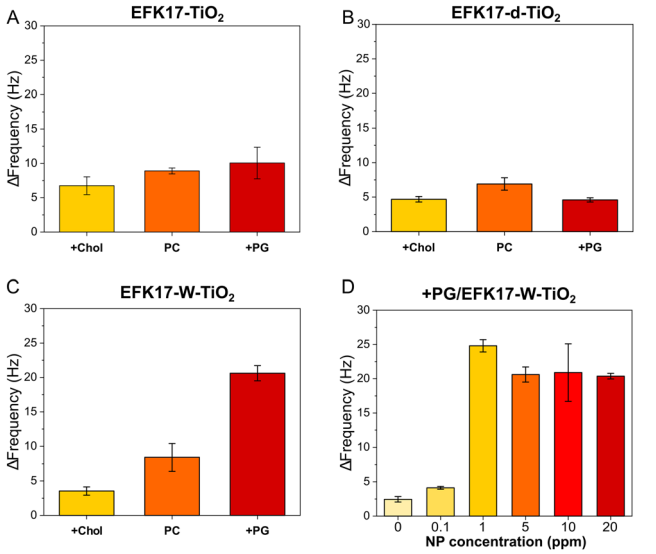

Fig. 4 QCM-d results showing frequency shifts caused by 2 h of *in situ* UV illumination on +Chol, PC, and +PG bilayers incubated with 5 ppm of EFK17-TiO_2 (A), EFK17-d-TiO_2 (B), and EFK17-W-TiO_2 (C). Shown in (D) are frequency shifts induced by 2 h of *in situ* UV illumination on +PG incubated with different concentrations EFK17-W-TiO_2. ΔF = 0 corresponds to the bilayer Frequency shift right before UV illumination. All measurements were performed in 10 mM acetate, pH 5.4. Representative QCM-d profiles for Fig. (A)–(C) are shown in Fig. S5 (EFK17-TiO_2), S6 (EFK17-d-TiO_2) and S7 (ESI†) (EFK17-W-TiO_2), while QCM-d kinetics corresponding to Fig. (D) are shown in Fig. S8 (ESI†) (n = 3).

differences in the size and surface charge of bare and peptide-coated TiO_2 (NPs). Quantitatively, however, the difference is very small, confirming that the peptide coatings have a minimal influence on ROS generation. Next, peptide conformational aspects were investigated by CD (Fig. 3A–D).

In line with previous results,[11] EFK17 (Fig. 3A) and EFK17-W (Fig. 3C) display disordered conformation in solution but pronounced helix formation after binding to anionic +PG LUVs. In contrast, EFK17-d (Fig. 3B) is unable to form the amphiphilic helix even in the presence of +PG LUVs. The latter applies also to EFK17-d in the presence of TiO_2 NPs and in the simultaneous presence of TiO_2 NPs and +PG LUVs. For both EFK17 and EFK17-W, on the other hand, the presence of either TiO_2 NPs or simultaneous presence of TiO_2 NP and +PG LUVs induce an increase in the helical conformation compared to the free peptide. Similar results were found for PC and +Chol LUVs (Fig. S2 and S3, ESI†).

UV-induced degradation of model membranes

The findings that relatively high peptide concentrations were needed to disperse TiO_2 NPs by EFK17-W, and that neither EFK17 nor EFK17-d was able to stabilize the TiO_2 NPs even at high peptide concentrations, suggest peptide-binding to the TiO_2 NPs was relatively weak. As a consequence, there is a risk of a fraction of the peptide added to TiO_2 NP dispersions being present as free peptides in solution. Considering this, the effects of free peptides on supported +PG bilayers were investigated (Fig. S4, ESI†). From QCM-d experiments, it was revealed that at a concentration <1.5 μM free peptides adsorb to the +PG bilayer (the extent of which depends on the peptide), without inducing any significant bilayer removal. Considering this, we selected an NP concentration of 5 ppm for the QCM-d experiments, corresponding to 2.5 μM peptide concentration, hence eliminating any effect of free peptide on membrane destabilization.

Results displayed in Fig. 4A–C show the photocatalytic effects of 5 ppm TiO_2 NPs coated with either EFK17 (A), EFK17-d (B), or EFK17-W (C), while corresponding QCM-d kinetics are reported in Fig. S5–S7 (ESI†).

As shown here, EFK17-W-TiO_2 displays potent photocatalytic degradation of bacteria-like +PG bilayers, whereas that of mammalian-like +Chol bilayers were much less degraded. EFK17-TiO_2 displays a similar dependence on the bilayer composition, although quantitatively, photocatalytic effects are significantly smaller than those of EFK17-W-TiO_2.

EFK17-d-TiO_2, finally, displays the smallest photocatalytic degradation, with results for +PG being essentially at the same level as bilayers in the absence of NPs or in the presence of bare TiO_2 NPs (Fig. S9, ESI†). Furthermore, Fig. 4D shows concentration effects for EFK17-W-TiO_2, with corresponding kinetics shown in Fig. S8 (ESI†). Altogether, these results show that (i) bare TiO_2 NPs (*i.e.*, zero peptide concentration) display very modest photocatalytic degradation (Fig. S9, ESI†), and (ii) photocatalytic degradation of +PG by EFK17-W-TiO_2 increases with the concentration of peptide-coated NPs at low particle concentrations, after which the effects saturate (Fig. 4D).

As discussed below, the latter is likely an effect of diffuse light scattering at high NP concentrations in the bilayer.

Structural aspects of lipid membrane degradation

To obtain structural information of UV-induced bilayer degradation, NR was performed for EFK17-W-TiO_2 NPs interacting with PC and +PG bilayers. Experiments were performed in 10 mM acetate buffer at pH 5.4, in three different contrasts, *i.e.* h-buffer, qm-buffer and d-buffer. NR profiles with best curve fits and corresponding SLD for bilayers before and after the addition of 20 ppm EFK17-W-TiO_2 NPs, as well as after 2 h of UV illumination, are shown in Fig. S10 (for the PC bilayer) and Fig. S11 (ESI†) (for the +PG bilayer). NR profiles acquired in different contrasts were fitted simultaneously to a 4-layer model (Scheme S1, ESI†), with input parameters summarized in Tables S1 and S2 (ESI†). To reduce the number of free parameters, the bilayer headgroup thickness was fixed at 7.5 Å.[34] PC and +PG bilayers before EFK17-W-TiO_2 NP addition were characterized by >99% coverage and ~0% tail hydration (Table S2, ESI†). Values of area per molecule (APM), headgroup hydration, bilayer thickness and surface coverage (Γ) were calculated as described previously[20] and are consistent with the previous literature[35,36] (Table S2, ESI†). Key structural parameters obtained from NR fits are shown in Fig. 5 and listed in Table S2 (ESI†).

With the exception of a modest decrease in the bilayer thickness (from 43 ± 1 Å before NP addition, to 39 ± 1 Å after NP addition, and to 37 ± 1 Å after UV illumination), no significant structural modification was detected for the PC bilayer upon EFK17-W-TiO_2 NP addition and UV illumination. Similarly, small structural changes were observed for +PG upon incubation with EFK17-W-TiO_2 in the absence of UV illumination, mainly consisting of a decrease in the bilayer thickness from 44 ± 1 Å to 37 ± 1 Å. In contrast, pronounced +PG destabilization was detected upon UV illumination. Specifically, a significant increase in the hydration of the acyl chains was observed (from 0.30 ± 0.01% to 34.0 ± 0.1%), mirrored by an overall increase of the area per molecule from 72 ± 4 $Å^2$ to 96 ± 4 $Å^2$. Similar increases in the hydration of bilayer tails and headgroups were previously observed for phosphatidylcholine membranes interacting with polystyrene nanoparticles bearing a soft protein corona shell.[37] In addition, the bilayer thickness decreased from 37 ± 1 $Å^2$ (before UV) to 34 ± 1 Å (after UV), paralleled by a significant lipid removal (Γ decreasing from 3.50 ± 0.05 mg m^{-2} to 2.60 ± 0.05 mg m^{-2}).

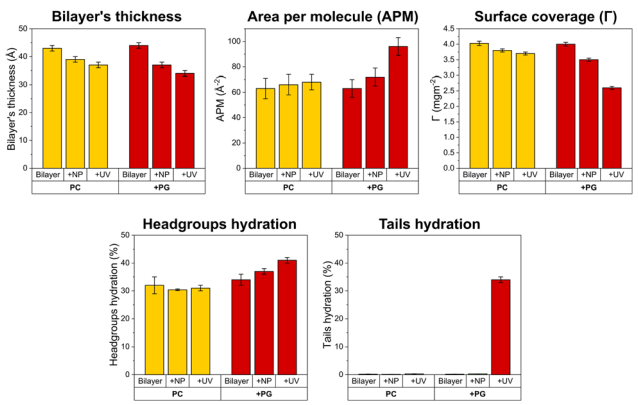

Fig. 5 Structural effects on supported PC and +PG bilayers incubated with 20 ppm EFK17-W-TiO_2 NPs. The reported parameters were extracted from NR fits for the system before NP incubation, after NP incubation, and after 2 h of *in situ* UV exposure. Shown are changes in bilayer thickness, area per lipid molecule (APM), surface coverage of the supported lipid bilayer (Γ), hydration of the hydrophilic headgroups, and hydration of the hydrophobic tails. Corresponding experimental curves, together with best fit curves and calculated SLD profiles, are shown in Fig. S10 (for the PC bilayer) and S11 (ESI†) (for the +PG bilayer).

Antibacterial effects

To investigate how results obtained in the bacteria-like model membranes correlated with antibacterial effects, we employed live/dead assay in combination with confocal microscopy. As presented in Fig. 6, both EFK17-TiO_2 and EFK17-W-TiO_2 killed bacteria already in darkness, mirroring the antimicrobial effect of free peptides.[11] In contrast, EFK17-d-TiO_2 displayed limited antimicrobial effect in darkness, again mirroring the effects of the free peptide in solution.[11] On UV exposure, some bacterial killing was observed under the conditions employed also for the bacterial suspension alone, reflecting the antimicrobial activity of UV illumination in the absence of TiO_2 NPs. In addition to this effect, however, the peptide-TiO_2 hybrid particles displayed boosted photocatalytic antimicrobial effects, particularly so for EFK17-W-TiO_2 and EFK17-TiO_2, whereas the antimicrobial effect under UV illumination for EFK17-d-TiO_2 was much smaller, and comparable to that in the absence of TiO_2 NPs.

Discussion

It has been well established in the literature that the affinity of various types of NPs for bacterial membranes can be increased by cationic surface modifications,[32] a consequence of bacterial membranes being rich in anionic phospholipids and lipopolysaccharides.[15,16] At the same time, however, cationic NPs are frequently toxic to human cells.[33,38,39] Considering that AMPs can be employed to achieve cationic surface modification, while also displaying selectivity between bacteria and human cells,[4,5,40] these have recently attracted interest as nanomaterial coatings in combatting infection.[40–43] Although such coatings may potentially be interesting for photocatalytic NPs,[3,41] the situation is more complex compared to non-photocatalytic NPs. For example, dense cationic coatings could prevent light-generated free electrons and holes from reaching the aqueous solution surrounding the NPs, therefore being unable to react with water, dissolved oxygen, and oxygen-containing solutes to form ROS. This should also apply to physisorbed peptide-based coatings, since the desorption of peptides is much slower than the ROS lifetime.[44,45] The absence of suppressed ROS generation in the present study indicates, however, that the surface coatings in the presently investigated systems including the EFK17-W layers, are

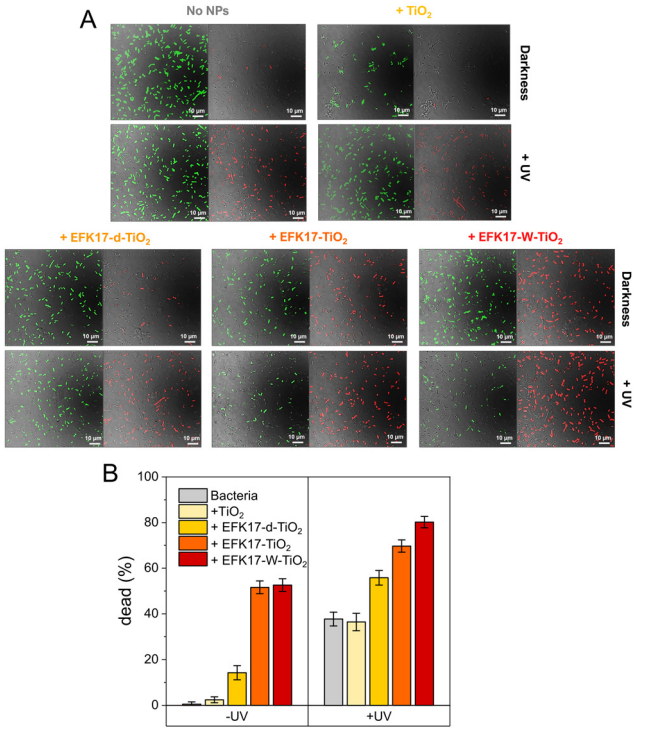

Fig. 6 (A) Representative confocal microscopy images obtained using live/dead assay (red, green, and Differential Interference Contrast images overlaid) for 10^8 CFU mL^{-1} of *E. coli* bacteria in 10 mM acetate, pH 5.4, without or with 1 h of incubation with bare TiO_2, EFK17-TiO_2, EFK17-d-TiO_2 or EFK17-W-TiO_2 with or without *in situ* UV illumination. For each system, live (green) and dead (red) bacteria are shown in separate images (left images for alive bacteria and right images for dead ones). (B) Quantification of confocal microscopy images, showing percentages of dead *E. coli* bacteria with or without UV illumination. Results are shown for bacteria alone and for bacteria exposed for 1 h to bare TiO_2, EFK17-TiO_2, EFK17-d-TiO_2 or EFK17-W-TiO_2 in 10 mM acetate, pH 5.4, with or without UV illumination (n = 3).

sufficiently "open" to allow free electrons and holes to form ROS at the TiO_2 NP surface. This is consistent with the high-water content observed for adsorbed polypeptide and protein layers,[46–49] as well as our previous findings relating to TiO_2 NPs coated with the AMP LL-37.[7] Another potential challenge with peptide-based surface coatings of photocatalytic NPs is that the peptide coating will ultimately degrade with extended ROS exposure. As shown by the modest change in ζ-potential of the peptide-coated NPs upon UV exposure in the present study, however, oxidative degradation is minor for at least 2 h of UV exposure. This is in line with our previous findings for TiO_2 NPs coated with the AMP LL-37.[7] Since the peptide-coated TiO_2 NPs remain positively charged during UV illumination for at least 2 h, they may bind extensively and preferentially to negatively charged bacterial membranes. In turn, this results in bacterial membrane disruption in darkness, which is strongly enhanced with UV illumination. This effect is supported by the short diffusion length required for generated ROS to reach their membrane target.

While we previously demonstrated that AMP-coating of TiO_2 NPs provides a way to boost antimicrobial effects while keeping toxicity against human cells low,[7] it remains unclear to what extent the properties of peptides in solution can be used as a guide to optimize this performance. In a first investigation into this, we recently studied the effects of hydrophobic end-tags on membrane interactions and antimicrobial effects of AMP-coated TiO_2 NPs.[8] By comparing the peptides KYE21 and WWWKYE21, for which the W-tag was previously demonstrated to strongly boost antimicrobial effects,[13] it was found that TiO_2 NPs coated with these peptides behave similarly, although WWWKYE21-TiO_2 binds much more extensively than KYE21-TiO_2 to bacteria-like +PG lipid bilayers. In addition, WWWKYE21-TiO_2 displayed similar membrane composition dependence as free WWWKYE21, binding more extensively to bacteria-like +PG bilayers than to mammalian-like +Chol bilayers. Since the selectivity between bacterial and mammalian cell membranes for the free peptides relates to effects of the membrane composition (anionic lipid and cholesterol content),[9,10] these results suggest that the W-residues in WWWKYE21 remain sufficiently exposed and mobile in WWWKYE21-TiO_2 to be able to interact with the lipid bilayer. Having said that, other mechanisms may contribute to membrane composition selectivity. For example, anionic phospholipids generally pack less densely than zwitterionic options,[35,36] which may facilitate particle insertion.[50,51] In addition, it has been suggested that anionic phospholipids undergo oxidative degradation differently as well.[52,53] Irrespectively, the dependence on lipid membrane composition was similar in that previous study (controlling peptide amphiphilicity by hydrophobic end-tags) to that observed in the present study (employing conformationally controlled peptide amphiphilicity).

An interesting feature of the present study is the dependence of photocatalytic degradation on nanoparticle concentration, showing a pronounced increase as a function of nanoparticle concentration before reaching a plateau (Fig. 4D). A similar effect was previously found for TiO_2 NPs coated with AMP WWWKYE21[8] and is likely due to diffuse light scattering by membrane-bound NPs deflecting some of the light, therefore resulting in less efficient ROS generation per particle at high local particle concentrations in the lipid bilayer.[54,55] Similar effects have been reported previously in photocatalytic degradation of organic toxins,[56] as well as for photolytic antibacterial effects.[57,58] This concentration dependence indicates that there is a limit for how far binding of peptide-coated photocatalytic NPs can be used to boost photocatalytic degradation.

Conclusions

Conformationally controlled amphiphilicity of antimicrobial peptides affects membrane interactions and antimicrobial effects of peptide-coated photocatalytic TiO_2 NPs, as summarized in Fig. 7. Specifically, we have demonstrated that coating TiO_2 NPs with the antimicrobial peptides EFK17, EFK17-d and EFK17-W does not significantly suppress ROS generation (Fig. 7A, left panel). Moreover, the peptide coatings display good stability towards UV-induced oxidative degradation (Fig. 7A, right panel). Remarkably, TiO_2 NPs coated with EFK17 and EFK17-W

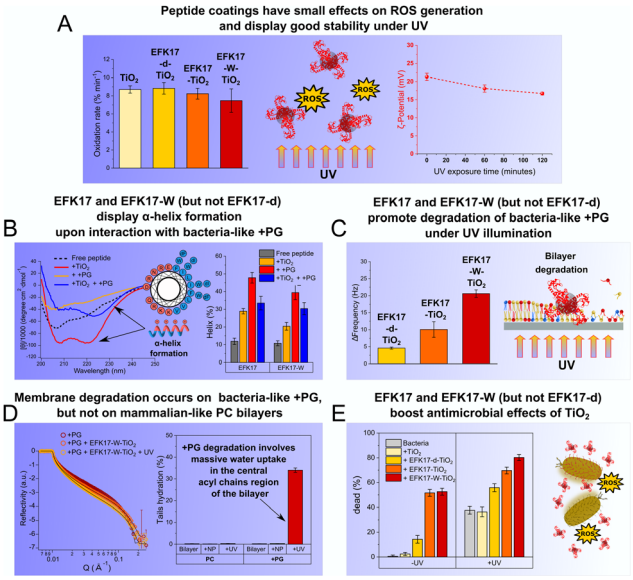

Fig. 7 Summary of the key findings of the study: conformationally controlled amphiphilicity of AMPs affects membrane interactions and antimicrobial effects of peptide-coated photocatalytic TiO_2 NPs. Demonstrating this, coating TiO_2 NPs with EFK17 and EFK17-W did not suppress ROS formation and displayed stability towards oxidative degradation for several hours (A). In addition, they displayed amphiphilic helix formation on bacterial membrane interaction (amphiphilicity being higher for EFK17-W than for EFK17 due to W substitutions) (B) and promoted degradation of bacteria-mimicking model bilayers compared to bare TiO_2 NPs (C), effects further enhanced on UV illumination and resulting ROS formation. NR results showed such membrane destabilization selectively occurs on bacteria-like +PG membranes (and not on mammalian-like PC bilayers) and involves water uptake in the hydrophobic chain region of the bilayer (D). In contrast, effects observed for EFK17-d, not forming such an amphiphilic helix, were substantially smaller. Demonstrating the effects observed in model lipid membranes to be relevant also for the biological effects of the peptide-coated NPs, confocal microscopy results on *E. coli* bacteria showed both EFK17-TiO_2 and EFK17-W-TiO_2, but not EFK17-d-TiO_2, to display pronounced antimicrobial effects already in darkness, effects further enhanced on UV illumination and ROS formation (E).

peptides, both displaying amphiphilic helix formation on bacterial membrane interaction (Fig. 7B), promoted higher degradation of bacteria-mimicking +PG bilayers compared to bare TiO_2 NPs. These effects were further enhanced with UV illumination due to the production of ROS adjacent to the membrane surface. (Fig. 7C). In contrast, TiO_2 NPs coated with EFK17-d, which did not form an amphiphilic helix upon interaction with bacteria-like +PG vesicles, induced significantly smaller membrane degradation (Fig. 7C). Similar to the behaviour of the free peptides, effects of EFK17-TiO_2 and EFK17-W-TiO_2 were significantly smaller on mammalian-like PC bilayers compared to bacteria-like +PG bilayers (Fig. 7D). Specifically, NR results revealed negligible structural changes of PC bilayers upon interaction with EFK17-W-TiO_2 NPs and subsequent UV illumination. In contrast, massive membrane destabilization was observed for +PG bilayers exposed to the same conditions, involving decreased membrane thickness and increased area per molecule, as well as the hydration of both headgroup and acyl chain regions (Fig. 7D). Finally, the effects of the peptide-coated NPs on *E. coli* bacteria showed both EFK17-TiO_2 and EFK17-W-TiO_2 to display pronounced antimicrobial effects, which could be further enhanced through ROS formation *via* UV illumination (Fig. 7E). Significantly smaller antimicrobial effects were observed for EFK17-W-TiO_2 or bare TiO_2 NPs (Fig. 7E). Taken together, the results from the study demonstrates that conformationally controlled AMP amphiphilicity, which dictates membrane interactions and antimicrobial effects of free AMPs in solution, apply also to peptide-coated photocatalytic NPs. The results also define a limit for such effects at high local membrane concentrations of NPs.

Author contributions

LC and MM designed the study. All authors were involved in performing the experiments and the interpretation of the experimental results. LC and MM wrote the paper. All authors reviewed the paper.

Conflicts of interest

There are no conflicts to declare.

Acknowledgements

We thank ILL for access to neutron beamtime and solid–liquid interface cells (Lucrezia Caselli; Ben Humphreys; Köhler Sebastian; Malmsten Martin and Schirone Davide. (2024). How do molecular properties of antimicrobial peptides influence bacterial membrane interactions of AMP-coated photocatalytic TiO_2 NPs? Institut Laue-Langevin (ILL) doi: **https://doi.org/10.5291/ILL-DATA.9-10-1805**). The research was funded by the Swedish Research Council (grant number 2021-05498; MM and LC), the Independent Research Fund Denmark (grant number 9040-00020B; MM and LC), and the LEO Foundation Center for Cutaneous Drug Delivery (grant number 15007; MM).

References

1 A. Gupta, S. Mumtaz, C.-H. Li, I. Hussain and V. Rotello, Combatting antibiotic-resistant bacteria using nanomaterials, *Chem. Soc. Rev.*, 2019, **48**, 415–427.
2 N.-Y. Lee, W.-C. Ko and P.-H. Hsueh, Nanoparticles in the treatment of infections caused by multidrug-resistant organisms, *Front. Pharmacol.*, 2019, **10**(1153), 1–10.
3 E. Parra-Ortiz and M. Malmsten, Photocatalytic nanoparticles – from membrane interactions to antimicrobial and antiviral effects, *Adv. Colloid Interface Sci.*, 2022, **102526**, 1–19.
4 T. Rončević, J. Puizina and A. Tossi, Antimicrobial peptides as anti-infective agents in pre-post-antibiotic era?, *Int. J. Mol. Sci.*, 2019, **20**(2713), 1–32.

5 R. E. W. Hancock, E. F. Haney and E. E. Gill, The immunology of host defence peptides: beyond antimicrobial activity, *Nat. Rev. Immunol.*, 2016, **16**, 321–334.
6 L. Martin, A. van Meegern, S. Doemming and T. Schuerholz, Antimicrobial peptides in human sepsis, *Front. Immunol.*, 2015, **6**(404), 1–7.
7 L. Caselli, E. Parra-Ortiz, S. Micciulla and M. Skoda, *et al.*, Boosting membrane interactions and antimicrobial effects of photocatalytic titanium dioxide nanoparticles by peptide coating, *Small*, 2024, 2309496.
8 L. Caselli, T. Traini, S. Micciulla, F. Sebastiani, *et al.*, Antimicrobial peptide coating of TiO2 nanoparticles for boosted antimicrobial effects, *ChemRxiv*, 2024, preprint, DOI: **10.26434/chemrxiv-2024-lb9hn**.
9 S. Singh, P. Papareddy, M. Kalle, A. Schmidtchen and M. Malmsten, Importance of lipopolysaccharide aggregate disruption for the anti-endotoxic effects of heparin cofactor II peptides, *Biochim. Biophys. Acta*, 2013, **1828**, 2709–2719.
10 S. Singh, A. Datta, A. Schmidtchen, A. Bhunia and M. Malmsten, Tryptophan end-tagging for promoted lipopolysaccharide interactions and anti-inflammatory effects, *Sci. Rep.*, 2017, **7**, 212.
11 A. A. Strömstedt, M. Pasupuleti, A. Schmidtchen and M. Malmsten, Evaluation of strategies for improving proteolytic resistance of antimicrobial peptides using variants of EFK17, an internal segment of LL-37, *Antimicrob. Agents Chemother.*, 2009, **53**, 539–602.
12 S. Singh, A. Datta, B. C. Borro, M. Davoudi, A. Schmidtchen, A. Bhunia and M. Malmsten, Conformational aspects of high content packing of antimicrobial peptides in polymer gels, *ACS Appl. Mater. Interfaces*, 2017, **9**, 40094–40106.
13 K. M. Reddy, S. V. Manorama and A. R. Reddy, Bandgap studies on anatase titanium dioxide nanoparticles, *Mater. Chem. Phys.*, 2003, **78**, 239–245.
14 J. Henriksen, A. C. Rowat, E. Brief, Y. W. Hsueh, J. L. Thewalt, M. J. Zuckermann and J. H. Ipsen, Universal behavior of membranes with sterols, *Biophys. J.*, 2006, **90**, 1639–1649.
15 C. W. Haest, J. de Gier, J. A. den Kamp, P. Bartels and L. L. van Deenen, Changes in permeability of Staphylococcus aureus and derived liposomes with varying lipid composition, *Biochim. Biophys. Acta*, 1972, **255**, 720–733.
16 R. F. Epand, P. B. Savage and R. M. Epand, Bacterial lipid composition and the antimicrobial efficacy of cationic steroid compounds (Ceragenins), *Biochim. Biophys. Acta*, 2007, **1768**, 2500–2509.
17 G. van Meer, Lipid traffic in animal cells, *Annu. Rev. Cell Biol.*, 1989, **5**, 247–275.
18 H. Lamberts, S. Piessens, A. Bloem, H. Pronk and P. Finkel, Natural skin surface pH is on average below 5, which is beneficial for its resident flora, *Int. J. Cosmet. Sci.*, 2006, **28**, 359–370.
19 E. Proksch, pH in nature, humans, and skin, *J. Dermatol.*, 2018, **45**, 1044–1052.
20 S. Malekkhaiat Häffner, E. Parra-Ortiz, M. W. A. Skoda, T. Saerbeck, K. L. Browning and M. Malmsten, Composition effects on photooxidative membrane destabilization, *J. Colloid Interface Sci.*, 2021, **584**, 19–33.
21 A. Micsonai, F. Wien, L. Kernya and Y. H. Lee, *et al.*, Accurate secondary structure prediction and fold recognition for circular dichroism spectroscopy, *Proc. Natl. Acad. Sci. U. S. A.*, 2015, **112**, E3095–E3103.
22 R. Cubitt and G. Fragneto, D17: The new reflectometer at the ILL, *Appl. Phys. A*, 2002, **74**, 329–331.
23 T. Saerbeck, R. Cubitt, A. Wildes, G. Manzin, K. H. Andersen and P. Gutfreund, Recent upgrades of the neutron reflectometer D17 at ILL, *J. Appl. Crystallogr.*, 2018, **51**, 249–256.
24 A. Nelson, Motofit – integrating neutron reflectometry acquisition, reduction and analysis into one, easy to use, package, *J. Phys.: Conf. Ser*, 2010, **251**, 012094.
25 A. Nelson, Co-refinement of multiple contrast neutron/X-ray reflectivity data using MOTOFIT, *J. Appl. Crystallogr.*, 2006, **39**, 273–276.
26 F. Heinrich, T. Ng, D. J. Vanderah, P. Shekar, M. Mihailescu, H. Nanda and M. Lösche, A new lipid anchor for sparsely tethered bilayer lipid membranes, *Langmuir*, 2009, **25**, 4219–4229.
27 L. Boulos, M. Prevost, B. Barbeau, J. Coallier and R. Desjardins, LIVE/DEAD® BacLight™: Application of a new rapid staining method for direct enumeration of viable and total bacteria in drinking water, *J. Microbiol. Methods*, 1999, **37**, 77–86.
28 C. A. Schneider, W. S. Rasband and K. W. Eliceiri, NIH Image to ImageJ: 25 years of image analysis, *Nat. Methods*, 2012, **9**(7), 671–675.
29 T. J. Collins, ImageJ for microscopy, *Biotechniques*, 2007, **43**(1 Suppl), 25–30.
30 M. Kosmulski, pH-dependent surface charging and points of zero charge: III. Update, *J. Colloid Interface Sci.*, 2006, **298**, 730–741.
31 M. Kosmulski, The significance of the difference in the point of zero charge between rutile and anatase, *Adv. Colloid Interface Sci.*, 2002, **99**, 255–264.
32 S. Malekkhaiat Häffner and M. Malmsten, Membrane interactions and antimicrobial effects of inorganic nanoparticles, *Adv. Colloid Interface Sci.*, 2017, **248**, 105–128.
33 N. Duran, C. P. Silveria, M. Duran and D. S. T. Martinez, Silver nanoparticle protein corona and toxicity: a mini-review, *J. Nanobiotechnol.*, 2015, **13**(55), 1–17.
34 J. Pan, F. A. Heberle, S. Tristram-Nagle, M. Szymanski, M. Koepfinger, J. Katsaras and N. Kučerka, Molecular structures of fluid phase phosphatidylglycerol bilayers as determined by small angle neutron and X-ray scattering, *Biochim. Biophys. Acta*, 2012, **1818**, 2135–2148.
35 G. Pabst, S. Danner, S. Karmakar, G. Deutsch and V. A. Raghunathan, On the propensity of phosphatidylglycerols to form interdigitated phases, *Biophys. J.*, 2007, **93**, 513–525.
36 N. Kučerka, F. A. Heberle, J. Pan and J. Katsaras, Structural significance of lipid diversity as studied by small angle neutron and X-ray scattering, *Membranes*, 2015, **5**, 454–472.
37 D. Di Silvio, M. Maccarini, R. Parker, A. Mackie, G. Fragneto and F. B. Bombelli, The effect of the protein corona on the

interaction between nanoparticles and lipid bilayers, *J. Colloid Interface Sci.*, 2017, **504**, 741–750.

38 K. I. McConnell, S. Shamsudeen, I. M. Meraz, T. S. Mahadevan, A. Ziemys, P. Rees, H. D. Summers and R. E. Serda, Reduced cationic nanoparticle toxicity based on serum masking of surface potential, *J. Biomed. Nanotechnol.*, 2016, **12**, 154–164.

39 M. Weiss, J. Fan, M. Claudel, T. Sonntag, P. Didier, C. Ronzani, L. Lebeau and F. Pons, Density of surface charge is a more predictive factor of the toxicity of cationic carbon nanoparticles than zeta potential, *J. Nanobiotechnol.*, 2021, **19**(5), 1–18.

40 C. Montis, E. Marelli, F. Valle, F. B. Bombelli and C. Pigliacelli, Engineering the interaction of short antimicrobial peptides with bacterial barriers, *Mol. Syst. Des. Eng.*, 2024, DOI: **10.1039/D4ME00021H**.

41 S. Malekkhaiat Häffner and M. Malmsten, Interplay between amphiphilic peptides and nanoparticles for selective membrane destabilization and antimicrobial effects, *Curr. Opin. Colloid Interface Sci.*, 2019, **44**, 59–71.

42 S. Malekkhaiat Häffner, E. Parra-Ortiz, K. L. Browning, E. Jørgensen, M. W. A. Skoda, C. Montis, X. Li, D. Berti, D. Zhao and M. Malmsten, Membrane interactions of virus-like mesoporous silica nanoparticles, *ACS Nano*, 2021, **15**, 6787–6800.

43 S. Malekkhaiat Häffner, L. Nyström, K. L. Browning, H. Mørck Nielsen, A. A. Strömstedt, M. J. A. van der Plas, A. Schmidtchen and M. Malmsten, Interaction of laponite with membrane compoents – Consequences for bacterial aggregation and infection confinement, *ACS Appl. Mater. Interfaces*, 2019, **11**, 15389–15400.

44 K. Das and A. Roychoudhury, Reactive oxygen species (ROS) and responses of antioxidants as ROS-scavengers during environmental stress in plants, *Front. Environ. Sci.*, 2014, **2**(53), 1–13.

45 F. Collin, Chemical basis of reactive oxygen species reactivity and involvement in neurodegenerative diseases, *Int. J. Mol. Sci.*, 2019, **20**(2407), 1–17.

46 D. Forciniti and W. A. Hamilton, Surface enrichment of proteins at quartz/water interfaces: a neutron reflectometry study, *J. Colloid Interface Sci.*, 2005, **285**, 458–468.

47 T. J. Su, J. R. Lu, R. K. Thomas, Z. F. Cui and J. Penfold, The effect of solution pH on the structure of lysozyme layers adsorbed at the silica-water interface studied by neutron reflectometry, *Langmuir*, 1998, **14**, 438–445.

48 B. M. Manzi, M. Werner, E. P. Ivanova, R. J. Crawford and V. A. Baulin, Simulations of protein adsorption on nanostructured surfaces, *Sci. Rep.*, 2019, **9**, 4694.

49 H. Min, E. Freeman, W. Zhang, C. Ashraf, D. Allara, A. C. T. Van Duin and S. Tadigadapa, Understanding kinetics of proteins adsorption at a liquid-solid interface, *Langmuir*, 2017, **33**, 7215–7224.

50 R. Michel and M. Gradzielski, Experimental aspects of colloidal interactions in mixed systems of liposome and inorganic nanoparticle and their applications, *Int. J. Mol. Sci.*, 2012, **13**, 11610–11642.

51 G. D. Bothun, N. Ganji, I. A. Khan, A. Xi and C. Bobba, Anionic and cationic silver nanoparticle binding restructures net-anionic PC/PG monolayers with saturated or unsaturated lipids, *Langmuir*, 2017, **33**, 353–360.

52 W. Y. Tai, Y. C. Yang, H. J. Lin, C. P. Huang, Y. L. Cheng, M. F. Chen, H. L. Yen and I. Liau, Interplay between structure and fluidity of model lipid membranes under oxidative attack, *J. Phys. Chem. B*, 2010, **114**, 15642–15649.

53 E. Schnitzer, I. Pinchuk and D. Lichtenberg, Peroxidation of liposomal lipids, *Eur. Biophys. J.*, 2007, **36**, 499–515.

54 P. Calza, M. Minella, L. Demarchis, F. Sordello and C. Minero, Photocatalytic dependence of light absorption properties of different TiO_2 specimens, *Catal. Today*, 2020, **340**, 12–18.

55 A. Tolosana-Moranchel, C. Pecharroman, M. Faraldos and A. Bahamonde, Strong effect of light scattering by distribution of TiO_2 particle aggregates on photocatalytic efficiency in aqueous suspensions, *Chem. Eng. J.*, 2021, **403**, 126186.

56 P. A. Mangrulkar, S. P. Kamble, M. M. Joshi, J. S. Meshram, N. K. Labhsetwar and S. S. Rayalu, Photocatalytic degradation of phenolics by N-doped mesoporous titania under solar radiation, *Int. J. Photoenergy*, 2012, **780562**, 1–10.

57 A. K. Benabbou, Z. Derriche, C. Felix, P. Lejeune and C. Guillard, Photocatalytic Inactivation of Escherichia coli: Effects of concentration of TiO_2 and microorganism, nature, and intensity of UV radiation, *Appl. Catal., B*, 2007, **76**, 257–263.

58 M. Karbasi, F. Karimzadeh, K. Raeissi, S. Rtimi, J. Kiwi, S. Giannakis and C. Pulgarin, insights into the photocatalytic bacterial inactivation by flower-like Bi_2WO_6 under solar or visible light, through in situ monitoring and determination of reactive oxygen species (ROS), *Water*, 2020, **12**, 1099.